Journal of Power Sources 220 (2012) 130–137

Contents lists available at SciVerse ScienceDirect

Journal of Power Sources

journal homepage: www.elsevier.com/locate/jpowsour

Electroless Ni–Cu–P/nano-graphite composite coatings for bipolar plates of proton exchange membrane fuel cells

Cheng-Kuo Lee*

Department of Mechanical Engineering, Chien Hsin University of Science and Technology, 229, Chien-Hsin Road, Chung-Li 32097, Taiwan, ROC

HIGHLIGHTS

- The 5083 alloy anodized at 10 °C improved the co-deposition and adhesion of electroless Ni–P–Cu composite coating.
- Adding the nanographite improved the electrical conductivity and corrosion resistance of the electroless Ni–Cu–P coating.
- Electroless Ni–Cu–P composite-coated 5083 aluminum alloy has great potential use as a bipolar plate in PEM fuel cells.

ARTICLE INFO

Article history:
Received 21 May 2012
Received in revised form
10 July 2012
Accepted 11 July 2012
Available online 7 August 2012

Keywords:
Electroless
Anodized
Nano-graphite
Corrosion
Fuel cell

ABSTRACT

This study evaluates the effects of an electroless Ni–Cu–P/nano-graphite composite coating on the surface characteristics of anodized 5083 aluminum alloy, including electrical resistivity, corrosion resistance of the alloy in a simulated solution of 0.5 M H_2SO_4 + 2 ppm NaF in polymer electrolyte membrane fuel cells (PEMFCs). The co-deposition and adhesion of the composite coatings on a 5083 substrate are enhanced by an anodizing process. The electroless Ni–Cu–P plating solution is prepared by adding different $CuSO_4 \cdot 5H_2O$ concentrations into the electroless Ni–P plating solution and adding nano-graphite (15–40 nm) particles to form the Ni–Cu–P/nano-graphite composite coatings. Experimental results indicate that the electroless Ni–Cu–P/nano-graphite composite coating enhances the hardness, conductivity, corrosion resistance of the 5083 substrate in the corrosive solution. The anodizing treatment enhances the electroless composite coatings by providing better uniformity, density, and adhesion compared to substrate without anodizing treatment. The electroless Ni–Cu–P/nano-graphite composite coating deposited on the optimal anodized 5083 substrate at a low $CuSO_4 \cdot 5H_2O$ concentration of 0.25 g l^{-1} with 20 g l^{-1} nano-graphite added have the best surface structure, highest hardness, electrical conductivity and corrosion resistance. Therefore, this novel electroless Ni–Cu–P/nano-graphite composite-coated 5083 aluminum alloy has potential applications in bipolar plates of PEM fuel cells.

1. Introduction

After the global oil crisis resulted in high fossil fuel prices and panic over fossil fuel depletion, researchers returned their attention to fuel cells. Fears of air pollution and global warming have been major contributors to the fuel cell renaissance. Proton exchange membrane fuel cells (PEMFCs) are considered one of the most promising fuel cell sources of fuel cell vehicles because they offer relatively high efficiency and power density. Moreover, PEMFCs provide a clean and reliable energy source that does not degrade the environment because they use hydrogen and oxygen (or air) to transform chemical energy into electric energy with water as the only byproduct. Therefore, researchers are intensively studying their materials to develop commercially viable applications that are competitive with other energy sources [1–5].

Bipolar plates have multiple important functions and are among the most expensive components in PEM fuel cell stacks [6–9]. Bipolar plates connecting individual fuel cell into stacks distribute fuel gas and oxygen to the anodes and cathodes of fuel cells and conduct current from one cell to another. However, bipolar plates are constantly exposed to a highly acidic solution containing cations of F^-, SO_4^{2-}, SO_3^{2-}, HSO^{-3}, CO_2^{-3} and HCO^{-3}, etc. [10]. These cations result from membrane dissolution and the electrode process technology. Therefore, the bipolar plates must resist reduction and oxidation to prevent the efficiency and lifetime of

* Tel.: +886 933946499; fax: +886 3 2503872.
E-mail address: cklee@uch.edu.tw.

0378-7753/$ – see front matter © 2012 Elsevier B.V. All rights reserved.
http://dx.doi.org/10.1016/j.jpowsour.2012.07.022

PEMFCs from degradation by interfacial contact resistance. Bipolar plates are usually fabricated from graphite because of its high electrical conductivity and corrosion resistance. However, because of the machining difficulty, the large volume, and the high cost of graphite, its commercial applications are limited [11–13]. A recent trend is the use of metallic bipolar plates instead because of their relatively low cost, good mechanical properties and the ease of machining the required fluid runner system, which enables smaller and thinner stacks [14–20]. However, unresolved problems include susceptibility to acidic corrosion and high contact electrical resistance caused by oxide and corrosion layers that form on the metal surfaces. The solutions are to increase the use of noble metals such as platinum or gold, which increases costs, or to use cheaper metals such as aluminum alloy and stainless steel, which require protective coatings. Some coated aluminum alloys have proven suitable candidates for bipolar plate materials because of their high corrosion resistance and stable PEM outputs [14,15,21,22].

One of the most promising coating technologies is electroless deposition, which is widely used for enhancing physical and mechanical properties such as corrosion and wear resistance of metallic materials. This autocatalytic process reduces metals and alloys without external power. Thus, the process is simple, fast, and inexpensive [23–26]. Moreover, electroless deposits have fine, dense and smooth surfaces with low porosity, which enable good substrate bonds. Due to their excellent wear and corrosion resistance and electrical conductivity, electroless Ni–P and Ni–B coatings are the most widely used coatings for under-bump metallization of flip chip packaging and for other applications in the chemical production industry. Coating properties can be further enhanced by including one or more metallic elements such as Cu, Co, Zn, Fe, Sn, W, Mo, *etc*. in the Ni–P matrix. Electroless nickel ternary alloy deposition is the most effective method of improving the physical and mechanical properties of binary Ni–P alloy systems [27,28]. Incorporating Cu into the Ni–P matrix substantially improves the coating microstructure and properties. Studies have confirmed that the thermal stability, magnetic and electrical properties, corrosion resistance and solderability of electroless Ni–Cu–P deposits are superior to those of electroless Ni–P deposits [29–31]. Therefore, electroless Ni–Cu–P alloys have potential applications as metallic bipolar plate coatings. Moreover, incorporating nano-sized particles in Ni–P autocatalytic coatings greatly improves their physical and chemical properties and confers new functional features that improve coating performance and enhance their applications in various fields [32]. Graphite, which has good electrical and thermal conductivity as well as good chemical stability, can be co-deposited with Cu [33], Ni [34], Ni–P [35,36], Cu–Zn [37], Cu–Sn [38,39] by electroless or electrolytic deposition to enhance tribological properties. However, the literature shows no reports of the effectiveness of graphite particle dispersed Ni–Cu–P ternary composite coatings applied on aluminum alloys for improving corrosion resistance and electrical conductivity of the substrate.

This study applied Ni–Cu–P/nanographite composite coatings on an anodized 5083 aluminum alloy substrate by electroless deposition under various concentrations of copper sulfate ($CuSO_4 \cdot 5H_2O$) and nanographite in the plating solution. Porous oxide film fabricated by anodizing method showed various surface morphologies as well as enhanced incorporation of ion species and particles from the plating solution, which enhanced electroless composite coatings formation. The effects of copper and graphite content on the hardness, electrical conductivity, corrosion behavior of the composite coatings in 0.5 M H_2SO_4 + 2 ppm NaF solution are investigated.

2. Experimental

2.1. Deposition of electroless Ni–Cu–P/nano-graphite composite coatings

The Ni–Cu–P/nano-graphite composite coatings were electroless deposited on Al–Mg alloy AA5083 substrates of bipolar plates (10 × 10 × 5 mm for wear corrosion measurements and 15 × 15 × 5 mm for electrochemical measurements) with the following chemical composition (wt.%): Si 0.04, Fe 0.03, Cu 0.08, Mn 0.7, Mg 4.7, Cr 0.15, Zn 0.20, Ti 0.10 and Al balance. The 5083 aluminum alloy is widely used in the automotive, marine, construction industries due to its high strength-to-weight ratio and superelasticity [40,41]. The presence of different kinds of intermetallic precipitates in the alloy matrix improves mechanical properties but decreases resistance to localized corrosion. The main intermetallic inclusions in the 5083 alloy are iron-rich and magnesium-rich intermetallics. The substrate surface was ground to 1200 grit emery paper and then polished with 1 and 0.05 μm Al_2O_3 powder pastes. Before performing the electroless deposition process, all specimens were pre-treated using the following process. Step one: wash specimens in 50 g l^{-1} NaOH solution at 70 °C for 30 s and rinse in deionized water. Step two: clean the specimens in 300 g l^{-1} HNO_3 solution at room temperature and then rinse by another immersion in deionized water. Step three: for comparison, anodize the specimens in 10% H_2SO_4 solution at various temperatures of 10 °C, 20 °C, 35 °C and 50 °C while applying 10 V for 1 h and stirring the solution at a constant rotation speed of 200 rpm. This anodizing treatment obtained the optimal porous substrate surface and enhanced the adhesion of subsequent electroless Ni–P–Cu/nano-graphite composite coatings [34]. Atomic force microscopy (AFM, Quesant Q-250CL) in contact mode was used to image the surface topography of the anodic layers. The average roughness (Ra) and root mean square roughness (RMS) parameters were measured in square regions with side lengths of 40 μm × 40 μm. Step four: perform zincating replacement of Zn by immersion in zincating solution of 120 g l^{-1} NaOH, 20 g l^{-1} ZnO, 1 g l^{-1} $NaNO_3$ and 50 g l^{-1} $C_3H_4(OH)(COOH)_3 \cdot H_2O$ two times for 30 s each.

The electroless Ni–P bath is composed of 15 g l^{-1} $NiSO_4 \cdot 6H_2O$, 15 g l^{-1} $NaH_2PO_2 \cdot H_2O$, 50 g l^{-1} $Na_3C_6H_5O_7 \cdot 2H_2O$ and 40 g l^{-1} NH_4Cl. The Ni–P–Cu alloy coatings were obtained by an electroless deposition process under various concentrations of 0.25 g l^{-1}, 0.5 g l^{-1} and 0.75 g l^{-1} $CuSO_4 \cdot 5H_2O$ added to the Ni–P solution. Various concentrations of 1 g l^{-1}, 5 g l^{-1}, 10 g l^{-1} and 20 g l^{-1} graphite nano-particles (average diameter, 15–40 nm) were then added to the Ni–Cu–P plating bath by 30 min ultrasonic dispersion. After immersion, the electroless process was performed to obtain the Ni–Cu–P/nano-graphite composite coating under magnetic agitation at a speed of 100 rpm and pH about 8.0 at temperature of 88 ± 1 °C for 1 h. After the electroless deposition process, the coated specimens were ultrasonically cleaned in deionized water.

2.2. Characterization of coatings

Coating surfaces, cross-sectional morphologies and compositions were characterized by scanning electron microscopy (SEM, JEOL JSM-6360) and X-ray energy dispersive spectrometry (EDS, INCA Energy 6587). Coating hardness was measured with a Vickers microhardness tester with a diamond tip and a maximum applied load of 500 g_f at an applied load of 100 g_f for 15 s. Three microhardness measurements were obtained for each sample, and the average value was recorded. The in-plane electrical resistivity of the coatings was measured using a four-point probe detecting system at room temperature and at a pin load of 100 g_f pin^{-1}. The through-

plane resistance was measured by using a technique similar to the method developed by Wang et al. [8]. Samples were placed between two carbon papers (Toray TGPH-120) to simulate the interfacial contact in a fuel cell stack. A compaction pressure of 2.0 MPa was applied by a universal testing machine (MTS810). A current of 2 A was applied by a DC power source supply (HP 3263A) through the two gold-coated copper plates, and the resultant voltages were monitored by a multimeter (Agilent 34420A). Coating resistivity was measured at five different locations on the sample, and the average resistivity was recorded.

2.3. Electrochemical and wear tests in 0.5 M H_2SO_4 + 2 ppm NaF solution

The corrosion resistance of the Ni–Cu–P/nanographite composite coatings in 0.5 M H_2SO_4 + 2 ppm NaF solution at 80 °C was measured by potentiodynamic polarization test. Potentiodynamic polarization test was performed by sweeping the potential from 0.25 V_{SCE} below open circuit potential (OCP) to 1.5 V_{SCE} at a scan rate of 1 mV s^{-1}. All potentials referred to the saturated calomel electrode (S.C.E.) and the auxiliary electrode was platinum. A potentiostat (EG & G Model 273A) and analysis software were used. The potentiostatic polarization test was also conducted at 0.6 V_{SCE} in the 0.5 M H_2SO_4 + 2 ppm NaF solution at 80 °C for 1 h to evaluate the corrosion resistance as a function of time.

3. Results and discussion

3.1. Anodic oxide film analysis

The oxide film of aluminum alloy formed by electrochemical anodic oxidation may exhibit a roughened surface with holes or cracks of various shape, size and number, which can affect mechanical properties. Nevertheless, the features of anodic oxide film are highly dependent on electrochemical anodic conditions. Because of its numerous fine holes and porous surface structure, the oxide film provides a useful interlayer for further electroless deposition. Therefore, to find the optimal porous oxide film, the 5083 substrate was anodized at various temperatures of 10 °C, 20 °C, 35 °C and 50 °C in 10% H_2SO_4 solution under an applied potential of 10 V and magnetic stirring at 100 rpm. Fig. 1 shows the results of SEM surface morphology observations and EDS analysis of the anodized layers that formed on the 5083 substrate at temperatures of 10 °C and 50 °C. Table 1 shows the surface hardness and film thickness of various anodized layers. Growth of the porous oxide film is associated with the formation of cracks as anodizing temperature increases from 10 °C to 35 °C. The oxide film hardness and thickness also correlate negatively with anodizing temperature (Table 1). The surface morphology of oxide film anodized at a low temperature of 10 °C exhibits a homogenous porous structure with numerous uniformly distributed holes (Fig. 1a). The EDS analysis shows the presence of both Al and O (Fig. 1b). This oxide film also has the highest hardness and film thickness (Table 1). As anodizing temperature increases to 50 °C, the anodizing reaction becomes too violent for anodic film formation, which results in major corrosion as detected by EDS analysis showing only pure Al element without any O detected. Table 1 also clearly shows that hardness decreases to 80.3 ± 3.0 Hv, which is lower than that of the substrate (81.3 ± 2.0 Hv).

The AFM results show that the surface roughness of the anodic film decreases as anodizing temperature increases. Table 2 shows the average roughness of Ra and RMS based on AFM images at a 40 μm × 40 μm sampling scale. The table clearly shows that both Ra and RMS decrease as anodizing temperature increases. Thus, the anodic oxide film anodized at a low temperature of 10 °C has the best roughing effect with the highest average roughness of Ra (912 nm) and RMS (763 nm). Fig. 2 shows the typical AFM images of the anodic film anodized at 10 °C, exhibiting a uniform porous structure with many small pores. Substrate pre-treatment is known to increase surface roughness and thus increase the number of active sites promoting co-absorption of ions and particles from the plating solution. This not only enhances the adsorption and growth of the electroless deposits on the substrate, it also increases compactness and density and decreases defects in the deposition layer. The corrosion resistance and tribological characteristics of the deposition layer are also enhanced [42,43]. Therefore, this condition is optimal used for the anodizing treatment of the substrate following for the electroless deposition.

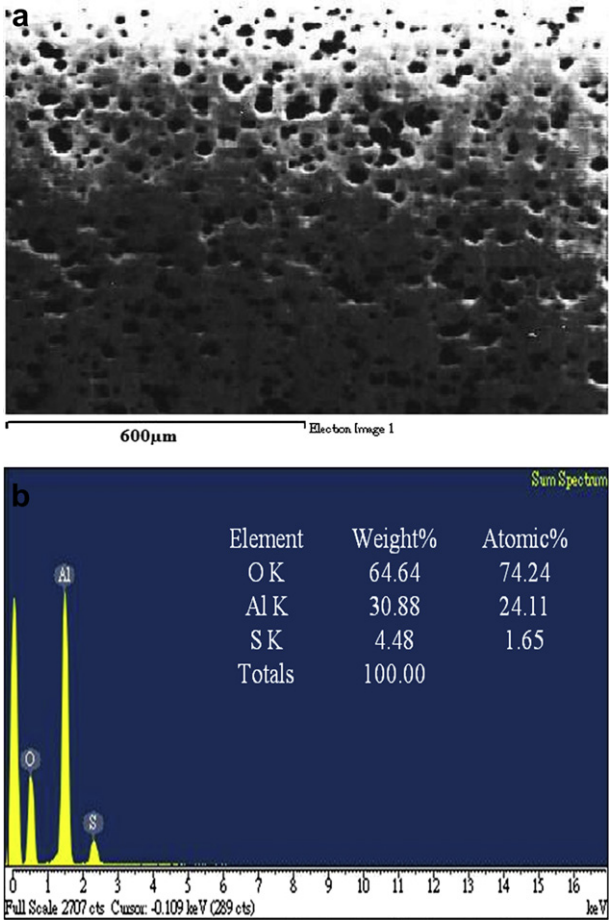

Fig. 1. (a) The SEM surface morphology and (b) EDS elemental analysis of 5083 aluminum alloy anodized in 10% H_2SO_4 solution at temperatures of 10 °C.

3.2. Characterization of the Ni–Cu–P/nano-graphite composite coatings

Theoretical models for describing the mechanisms of particle entrapment in the deposition process have been based on studies

Table 1
Surface hardness and film thickness of the aluminum oxide anodizing at various temperatures.

Film property	Anodizing temperature			
	10 °C	20 °C	30 °C	50 °C
Hardness (Hv)	93.1 ± 5.0	87.1 ± 4.0	83.1 ± 5.0	80.3 ± 3.0
Film thickness (μm)	4.24 ± 0.04	3.30 ± 0.03	2.50 ± 0.02	–

Table 2
Roughness parameters Ra and RMS of aluminum oxide anodizing at various temperatures.

Film property	Anodizing temperature			
	10 °C	20 °C	30 °C	50 °C
RMS (nm)	763.2	356.4	202.7	175.1
Ra (nm)	912.5	217.1	156.3	103.5

by Guglielmi [44]. Particles are co-deposited by a two-step adsorption mechanism. The first step transports the dispersed particles in the plating bath to the electrode surface by mechanical action and by physical adsorption in fluidal attack. In the second step these physically adsorbed particles are dehydrated by the strong electric field of the Helmholtz layer of the electrode, and a strong irreversible chemical adsorption of particles on the electrode occurs. The adsorbed particles are embedded by reduced metal or alloys [45].

Morphological analyses of the Ni–Cu–P/nano-graphite composite coating surfaces show that irregularities, coarseness and nano-graphite aggregation increase as nano-graphite particles are added to solutions with increasing concentrations of $Cu_2SO_4 \cdot 5H_2O$ from 0.25 g l^{-1} to 0.75 g l^{-1}. Fig. 3 shows the surface and cross-sectional SEM images and EDS analysis of the Ni–Cu–P/nano-graphite composite coatings electroless deposited in the solution containing 0.25 g l^{-1} $Cu_2SO_4 \cdot 5H_2O$ and 20 g l^{-1} nano-graphite particles. The aggregation of many small round particles is uniform in this Ni–Cu–P/nano-graphite composite coating (Fig. 3a). The cross-sectional image reveals that the Ni–Cu–P/nano-graphite composite coating is compatible with the 5083 aluminum substrate with no interfacial defects between the coating and substrate. The coating has a thickness of about 45.8 ± 0.6 μm, which is much thicker than the coating without added nano-graphite, *i.e.*, the Ni–Cu–P coating (8.50 ± 0.05 μm) (Fig. 3b). The beneficial effect of adding nano-sized particles in the plating solution is the promotion of coating growth due to its superior co-deposition competing against other ions. The EDS analysis revealed Ni, P, Cu and C in the composite coating (Fig. 3c). When 0.75 g l^{-1} $Cu_2SO_4 \cdot 5H_2O$ is added, pits and holes gradually appear on the composite coating surface due to the decreased absorption of ions and particles as the nano-graphite concentration in the solution increases. Fig. 4 shows the surface morphology and EDS analysis of the composite coatings electroless deposited in the solution containing 0.75 g l^{-1} $Cu_2SO_4 \cdot 5H_2O$ and 20 g l^{-1} nano-graphite particles. Numerous pits, holes and cracks are clearly visible in this composite coating. The O and Al in the substrate revealed by EDS indicate a fracture in the composite coating. Fig. 5 shows the results of EDS analysis of carbon content in various electroless Ni–Cu–P/nano-graphite composite coatings. The carbon content existing in the composite coatings deposited in the solution containing $Cu_2SO_4 \cdot 5H_2O$ concentration from 0.25 g l^{-1} to 0.50 g l^{-1}, is increased with the added amount of nano-graphite particles in the solution. When $Cu_2SO_4 \cdot 5H_2O$ concentration is increased to 0.75 g l^{-1}, carbon content significantly decreases. The experimental results suggest that the nano-graphite particle has a superior competing effect of deposition compared to the other ions at a low $Cu_2SO_4 \cdot 5H_2O$ concentration of 0.25 g l^{-1} and obtains the highest carbon content in the composite coating.

Fig. 6 indicates the average micro-hardness of various electroless Ni–Cu–P/nano-graphite composite coatings. The figure clearly shows that, at a low $Cu_2SO_4 \cdot 5H_2O$ concentration of 0.25 g l^{-1}, the nano-graphite particle has a superior competing effect of deposition compared to the other ions. Accordingly, the surface hardness of the composite coatings electroless deposited in the solution containing 0.25 g l^{-1} and 0.50 g l^{-1} $Cu_2SO_4 \cdot 5H_2O$ concentration. The figure clearly shows that, at a low $Cu_2SO_4 \cdot 5H_2O$ concentration of 0.25 g l^{-1}, the nano-graphite particle has a superior competing effect of deposition compared to the other ions nano-graphite concentration. However, at 0.75 g l^{-1} $Cu_2SO_4 \cdot 5H_2O$ concentration, the hardness of the composite coating significantly decreases as the nano-graphite concentration increases. The experimental results confirm that the hardness of the composite coatings at 0.25 g l^{-1} and 0.50 g $l^{-1}$$Cu_2SO_4 \cdot 5H_2O$ increases as nano-graphite is added because the co-deposited nano-graphite particles in the coatings have a particle dispersion strengthening effect [46].

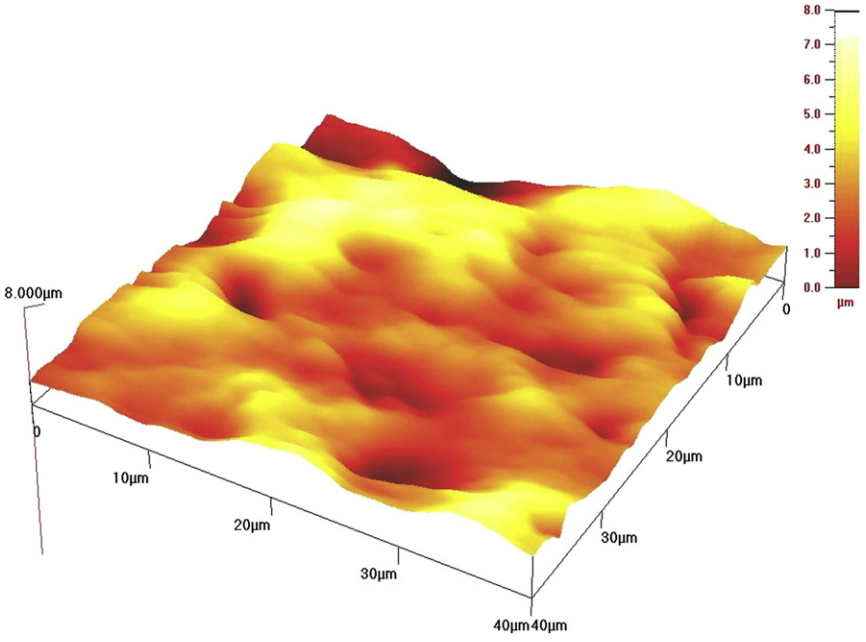

Fig. 2. The AFM images of 5083 aluminum alloy anodized in 10% H_2SO_4 solution at temperature of 10 °C.

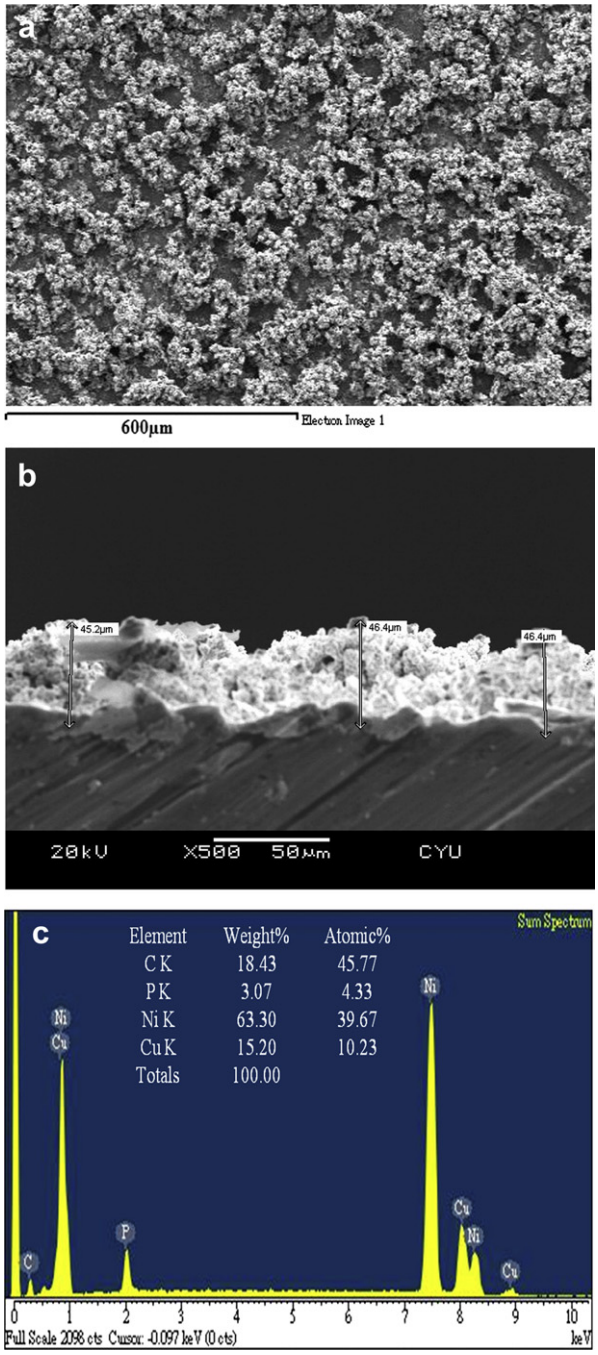

Fig. 3. The SEM images of (a) surface and (b) cross-sectional morphology, and (c) EDS elemental analysis of the electroless Ni–Cu–P/nanographite composite coating prepared in plating solution containing 0.25 g l^{-1} $CuSO_4 \cdot 5H_2O$ and 20 g l^{-1} nano-graphite.

Fig. 7 shows the in-plane electrical resistivity (Fig. 7(a)) and through-plane resistance (Fig. 7(b)) of the electroless Ni–Cu–P/nano-graphite composite coatings observed under various conditions. Both in-plane electrical resistivity and through-plane resistance significantly decrease as nano-graphite particles are added in the coatings prepared in the solution at 0.25 g l^{-1} and 0.50 g l^{-1} $Cu_2SO_4 \cdot 5H_2O$ concentration. Specifically, when the nano-graphite concentration is increased to 20 g l^{-1}, the coatings prepared in the solution at 0.25 g l^{-1} and 0.50 g l^{-1} $Cu_2SO_4 \cdot 5H_2O$ concentration, they have quite low in-plane electrical resistivity of 30.0 ± 4.8 μΩ cm and 28.0 ± 4.0 μΩ cm and through-plane resistance of 8.5 ± 0.8 mΩ cm^2

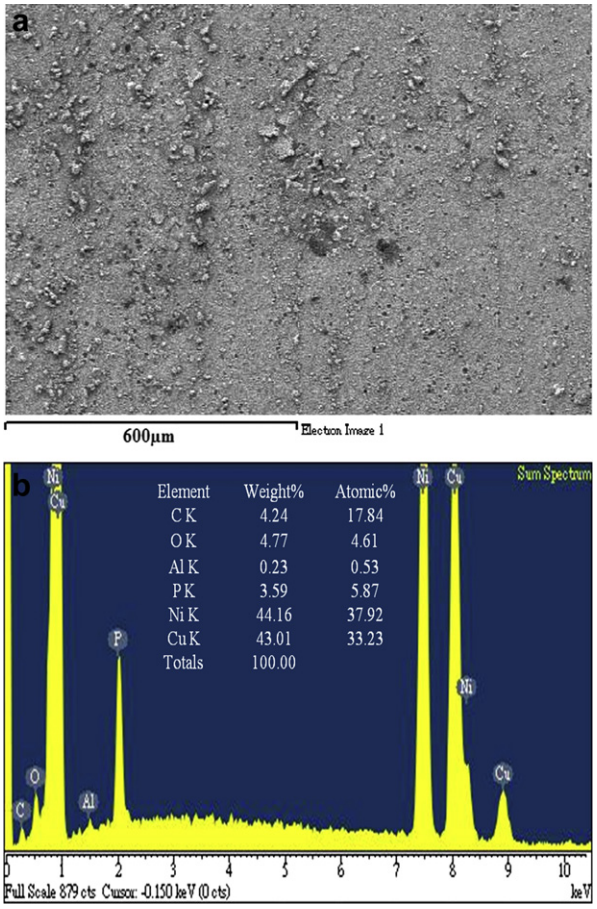

Fig. 4. The SEM images of (a) surface morphology and (b) EDS elemental analysis of the electroless Ni–Cu–P/nanographite composite coating prepared in plating solution containing 0.75 g l^{-1} $CuSO_4 \cdot 5H_2O$ and 20 g l^{-1} nano-graphite.

and 8.0 ± 0.5 mΩ cm^2, respectively. These two electrical properties can meet the U.S. Department of Energy (DOE) 2020 technical targets, which indicating the in-plane electrical conductivity >100 S cm^{-1} and areal specific resistance of 0.01 Ω cm^2, respectively for bipolar plates of PEMFCs [47]. However, in the coating prepared in the solution at 0.75 g l^{-1} $Cu_2SO_4 \cdot 5H_2O$ concentration, these two electrical properties increase with nano-graphite concentration because of the imperfect and fragmented coating (Fig. 4).

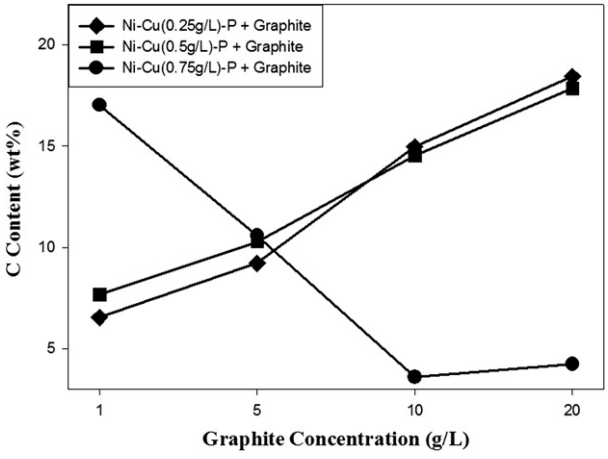

Fig. 5. Carbon content in the electroless Ni–Cu–P/nano-graphite composite coatings.

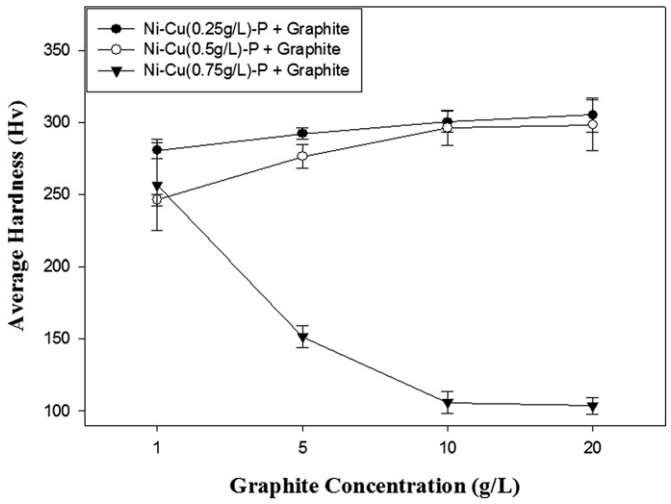

Fig. 6. Average micro-hardness values of the electroless Ni–Cu–P/nano-graphite composite coatings.

3.3. Electrochemical corrosion behavior

An aqueous 0.5 M H_2SO_4 + 2 ppm NaF solution was used as a corrosion electrolyte to evaluate the corrosion resistance of the composite coatings. Figs. 8–10 show the potentiodynamic polarization curves for various composite coatings. The figures clearly show that all electroless Ni–Cu–P/nano-graphite composite coatings exhibit a superior electrochemical corrosion behavior, *i.e.*, the anodic polarization curve shifts toward to the left side of corrosion current, and the corrosion potential moves upward to a more noble direction compared to the 5083 substrate, as nano-graphite is added to the plating solution. The corrosion current density of the 5083 aluminum is about 1.71×10^{-4} A cm^{-2}, which confirms the inferior corrosion resistance of the aluminum alloy. Because 2 ppm NaF was added, this value, which was obtained in the test of 0.5 M H_2SO_4 solution, exceeds that reported in a previous study [48]. However, the polarization curves for the coating prepared in a solution with a $Cu_2SO_4 \cdot 5H_2O$ concentration of 0.75 g l^{-1} cannot be measured when the concentration of added nano-graphite exceeds 1 g l^{-1} because of fractures and imperfections in the coating. The corrosion current density was determined

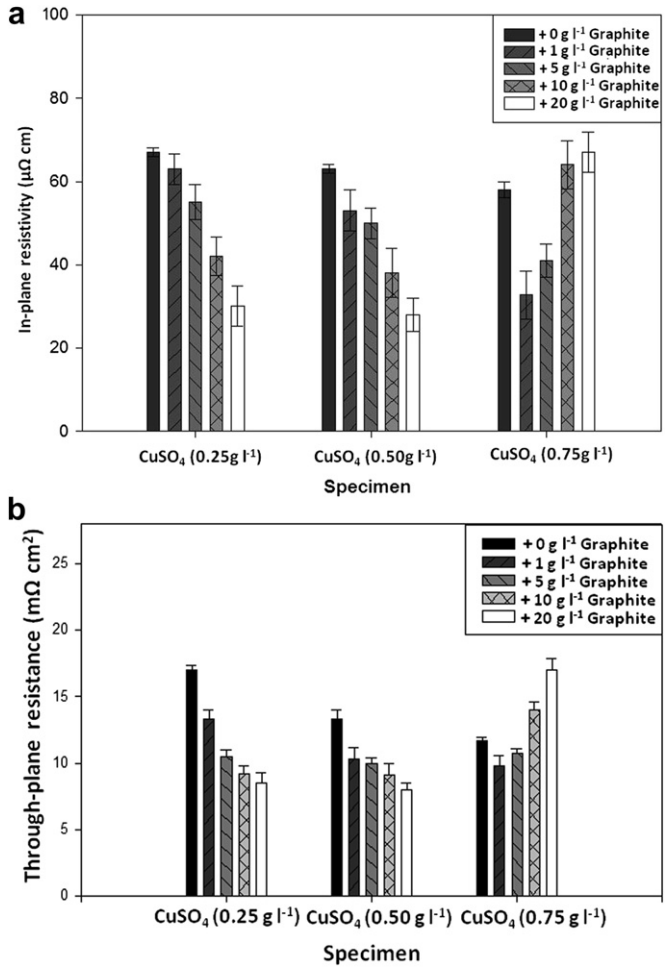

Fig. 7. (a) In-plane electrical resistivity and (b) through-plane resistance values of the electroless Ni–Cu–P/nano-graphite composite coatings.

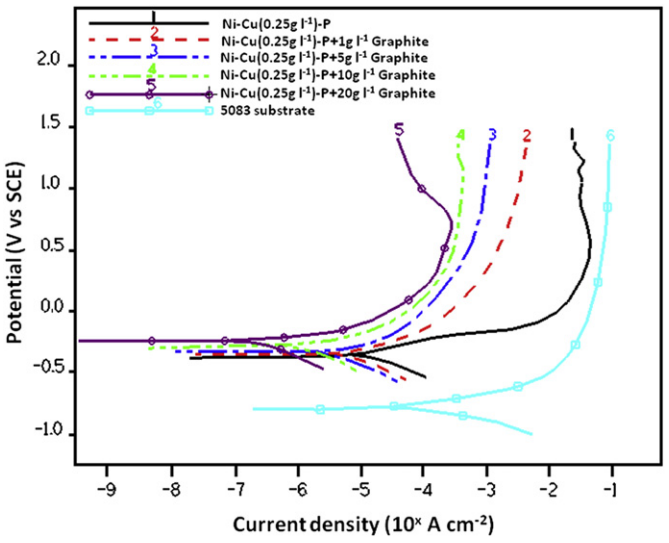

Fig. 8. Potentiodynamic polarization curves tested in 0.5 M H_2SO_4 + 2 ppm NaF at 80 °C for the electroless Ni–Cu–P/nano-graphite composite coating prepared in plating solution containing 0.25 g l^{-1} $CuSO_4 \cdot 5H_2O$ at various nano-graphite concentrations.

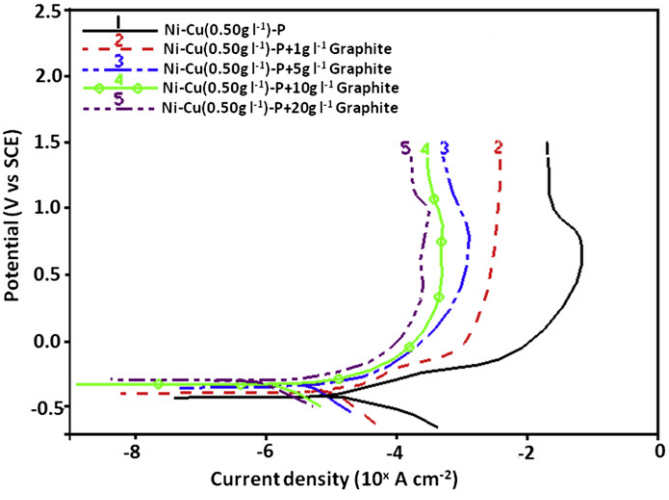

Fig. 9. Potentiodynamic polarization curves tested in 0.5 M H_2SO_4 + 2 ppm NaF at 80 °C for the electroless Ni–Cu–P/nano-graphite composite coating prepared in plating solution containing 0.50 g l^{-1} $CuSO_4 \cdot 5H_2O$ at various nano-graphite concentrations.

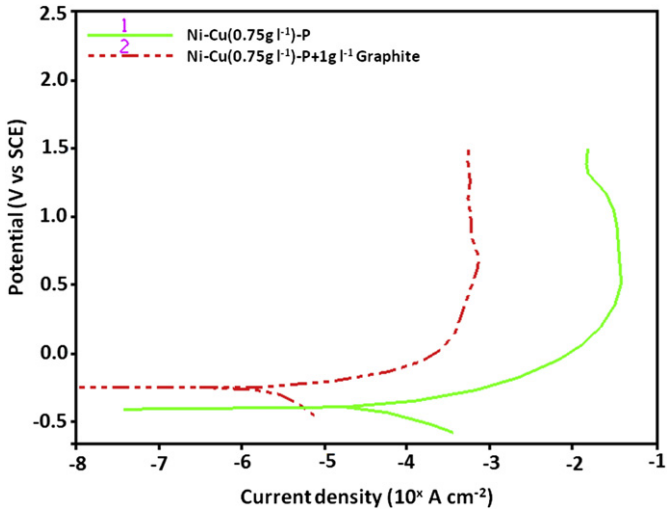

Fig. 10. Potentiodynamic polarization curves tested in 0.5 M H_2SO_4 + 2 ppm NaF at 80 °C for the electroless Ni–Cu–P/nano-graphite composite coating prepared in plating solution containing 0.75 g l^{-1} $CuSO_4{\cdot}5H_2O$ at various nano-graphite concentrations.

by extrapolating the rectilinear Tafel segments of the anode and cathode polarization curves. The polarization resistance values were determined by the equation $i_{corr} = \beta/R_p$ where β is a constant calculated by the following equation:

$$\beta = \beta_a \cdot \beta_c / 2.3(\beta_a + \beta_c) \quad (1)$$

where β_a and β_c are the anodic and cathodic Tafel slopes, respectively, obtained from polarization curves.

Tables 3–5 show the corrosion potential (E_{corr}), corrosion current density (i_{corr}) and polarization resistance (R_p) obtained from the polarization curves. Comparison of these tables clearly shows that, at the highest added nano-graphite concentration of 20 g l^{-1}, the electroless Ni–Cu–P/nano-graphite composite coating prepared in the 0.25 g l^{-1} $Cu_2SO_4{\cdot}5H_2O$ solution has the best corrosion resistance, the lowest corrosion current density of 0.24 μA cm^{-2}, the most noble corrosion potential of −244.2 mV_{SCE}, and the highest polarization resistance of 8.56 kΩ cm^2. This corrosion current is also superior to the 1 μA cm^{-2} corrosion current required by the U.S. DOE 2020 technical targets for bipolar plates of PEMFCs [47]. This improvement was achieved by the enhanced electroless co-deposition provided by the nano-graphite in the composite coating prepared in the solution containing lower $Cu_2SO_4{\cdot}5H_2O$ concentration of 0.25 g l^{-1}. Because of its high chemical stability, the electroless Ni–Cu–P/nano-graphite composite coating incorporated more nano-graphite, which significantly improved the corrosion resistance of the coating. In the presence of graphite micro-cell formation increases, because the graphite in micro-cells acts as a cathode and nickel acts as anode, the standard potential of graphite is more positive than that caused by nickel corrosion of micro-cells. Therefore, anodic polarization is facilitated, and localized corrosion is inhibited. That is, corrosion is mainly homogenous as indicated in Fig. 9 [49]. In the case of electroless composite coating, incorporating nano-graphite particles in the composite coating also considerably decreases the effective metallic area prone to corrosion.

Further evidence of the corrosion resistance is seen in the potentiostatic polarization results shown in Fig. 11, where the polarization potential of 0.6 V_{SCE} is considered as a typical cathodic potential under the PEFC environment. The observed current density of the 5083 substrate is significantly higher than that of the electroless Ni–Cu–P/nano-graphite composite coatings. The current density of the electroless Ni–Cu–P/nano-graphite composite coatings also decreases with the added nano-graphite concentration. The current density of electroless Ni–Cu(0.25 g l^{-1})–P added the highest nano-graphite concentration of 20 g l^{-1} possesses the lowest value of 0.819 μA cm^{-2}, which is also well below the recommended upper limit value of 1 μA cm^{-2}

Table 3
Electrochemical characteristics of the electroless Ni–Cu–P/nano-graphite composite coating prepared in plating solution containing 0.25 g l^{-1} $CuSO_4{\cdot}5H_2O_4$ with various concentrations of nano-graphites.

Specimen (0.25 g l^{-1} $CuSO_4{\cdot}5H_2O$)	E_{corr} (mV_{SCE})	i_{corr} (μA cm^{-2})	R_p (kΩ cm^2)
0 g l^{-1} nanographite	−395.3	12.20	0.32
1 g l^{-1} nanographite	−353.5	8.41	0.53
5 g l^{-1} nanographite	−325.6	4.02	2.73
10 g l^{-1} nanographite	−281.4	0.94	5.94
20 g l^{-1} nanographite	−244.2	0.24	8.56

Table 4
Electrochemical characteristics of the electroless Ni–Cu–P/nano-graphite composite coating prepared in plating solution containing 0.50 g l^{-1} $CuSO_4{\cdot}5H_2O$ with various concentrations of nano-graphites.

Specimen (0.50 g l^{-1} $CuSO_4{\cdot}5H_2O$)	E_{corr} (mV_{SCE})	i_{corr} (μA cm^{-2})	R_p (kΩ cm^2)
0 g l^{-1} nanographite	−433.3	14.82	1.85
1 g l^{-1} nanographite	−406.3	11.10	0.80
5 g l^{-1} nanographite	−356.3	5.41	3.84
10 g l^{-1} nanographite	−333.3	1.91	5.77
20 g l^{-1} nanographite	−291.7	0.78	6.01

Table 5
Electrochemical characteristics of the electroless Ni–Cu–P/nano-graphite composite coating prepared in plating solution containing 0.75 g l^{-1} $CuSO_4{\cdot}5H_2O$ with various concentrations of nano-graphites.

Specimen (0.75 g l^{-1} $CuSO_4{\cdot}5H_2O$)	E_{corr} (mV_{SCE})	i_{corr} (μA cm^{-2})	R_p (kΩ cm^2)
0 g l^{-1} nanographite	−392.2	44.10	0.12
1 g l^{-1} nanographite	−255.1	2.08	5.26
5 g l^{-1} nanographite	–	–	–
10 g l^{-1} nanographite	–	–	–
20 g l^{-1} nanographite	–	–	–

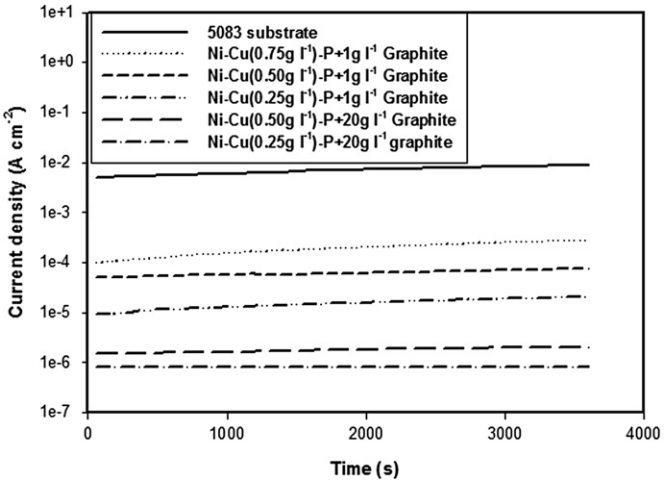

Fig. 11. Potentiostatic curves of the samples polarized at 0.6 V_{SCE} in the 0.5 M H_2SO_4 + 2 ppm NaF at 80 °C for 1 h.

by the U.S. DOE 2020 technical targets for bipolar plates of PEMFCs [47]. These experimental results indicate that the electroless Ni–Cu–P/nanographite composite coatings prepared in the solution of 0.25 g l^{-1} $CuSO_4 \cdot 5H_2O$ and 20 g l^{-1} nano-graphite concentrations provide excellent corrosion protection for the 5083 aluminum substrate. Consequently, this composite-coated aluminum alloy may have potential applications used as a bipolar plate in the PEMFCs even concerning the service life in severe corrosive solution.

4. Conclusions

(1) The 5083 aluminum alloy anodized at a low temperature of 10 °C provided a fine porous oxide film with the highest hardness. The benefits of this roughing surface included improvement of the co-deposition and adhesion of electroless Ni–Ci–P/nanographite composite coating on the aluminum alloy substrate.
(2) Adding the nanographite to the electroless Ni–Cu–P plating solution showed that the nanographite codeposited well at the $Cu_2SO_4 \cdot 5H_2O$ concentration below 0.75 g l^{-1}. Moreover, the carbon content in the composite coating significantly increased with the addition of nanographite.
(3) Adding the nanographite improved the electrical conductivity of the electroless Ni–Cu–P coating, which increased the corrosion protection provided by the Ni–Cu–P/nano-graphite composite coating on the 5083 aluminum substrate in 0.5 M H_2SO_4 + 2 ppm NaF solution.
(4) The electroless Ni–Cu–P/nanographite composite coating deposited on the optimal anodized 5083 aluminum alloy substrate with a low $Cu_2SO_4 \cdot 5H_2O$ concentration of 0.25 g l^{-1} with 20 g l^{-1} nanographite added had the best surface structure, hardness, electrical conductivity, corrosion resistance in the corrosive solution of PEMFCs. Therefore, this novel electroless Ni–Cu–P/nanographite composite coated 5083 aluminum alloy has great potential use as a bipolar plate in PEM fuel cells.

Acknowledgments

The author would like to thank the National Science Council of the Republic of China, Taiwan, for financially supporting this research under Contract No. NSC-100-2622-E-231-001-CC3.

References

[1] L. Wang, D.O. Northwood, X. Nie, J. Housden, E. Spain, A. Leyland, A. Matthews, Journal of Power Sources 195 (2010) 3814–3821.
[2] D. Zhang, L. Duan, L. Guo, W.H. Tuan, International Journal of Hydrogen Energy 35 (2010) 3721–3726.
[3] A.E. Fetohi, R.M. Abdel Hameed, K.M. El-Khatib, Eglal R. Souaya, International Journal of Hydrogen Energy 37 (2011) 7677–7688.
[4] H. Tawfik, Y. Hung, D. Mahajan, Journal of Power Sources 163 (2007) 755–767.
[5] Y.Y. Shao, G.P. Yin, Z.B. Wang, Y.Z. Gao, Journal of Power Sources 167 (2007) 235–242.
[6] A. Hermann, T. Chaudhuri, P. Spagnol, International Journal of Hydrogen Energy 30 (2005) 1297–1302.
[7] H. Chen, H.B. Liu, L. Yang, J.X. Li, International Journal of Hydrogen Energy 35 (2010) 3105–3109.
[8] H.L. Wang, M.A. Sweikart, J.A. Turner, Journal of Power Sources 115 (2003) 243–251.
[9] B. Cunningham, D.G. Baird, Journal of Materials Chemistry 16 (2006) 4385–4388.
[10] R. Tian, J. Sun, L. Wang, International Journal of Hydrogen Energy 31 (2006) 1874–1878.
[11] I.E. Paulauskas, M.P. Brady, H.M. Meyer III, R.A. Buchanan, L.R. Walker, Corrosion Science 48 (10) (2006) 3157–3171.
[12] I.U. Hwang, H.N. Yu, S.S. Kim, D.G. Lee, J.D. Suh, S.H. Lee, B.K. Ahn, S.H. Kim, T.W. Lim, Journal of Power Sources 184 (2008) 90–94.
[13] V. Mehta, J.S. Cooper, Journal of Power Sources 114 (1) (2003) 32–53.
[14] A.E. Fetohi, R.M. Abdel Hameed, K.M. El-Khatib, E.R. Souaya, International Journal of Hydrogen Energy 37 (2012) 7677–7688.
[15] C.Y. Bai, Y.H. Chou, C.L. Chao, S.J. Lee, M.G. Ger, Journal of Power Sources 183 (2008) 174–181.
[16] T. Fukutsuka, T. Yamagichii, S.I. Miyano, Y. Matsuo, Y. Sugie, Z. Ogumi, Journal of Power Sources 174 (2007) 199–205.
[17] Y. Show, Surface and Coatings Technology 202 (2007) 1252–1255.
[18] M.C. Li, S.Z. Luo, C.L. Zeng, J.N. Shen, H.C. Lin, C.N. Cao, Corrosion Science 46 (2004) 1369–1380.
[19] Y. Wang, D.O. Northwood, Journal of Power Sources 165 (2007) 293–298.
[20] J. Wang, J. Sun, S. Li, Z. Wena, S. Ji, International Journal of Hydrogen Energy 37 (2012) 1140–1144.
[21] Y. Hung, K.M. El-khatib, H. Tawfik, Journal of Power Sources 163 (2006) 509–513.
[22] J. Wind, R. Spah, W. Kaiser, G. Bohm, Journal of Power Sources 105 (2002) 256–260.
[23] X.C. Wang, W.B. Cai, W.J. Wang, H.T. Liu, Z.Z. Yu, Surface and Coatings Technology 168 (2003) 300–306.
[24] J.W. Schultze, A. Bressel, Electrochimica Acta 47 (2001) 3–21.
[25] C.K. Chen, H.M. Feng, H.C. Lin, M.H. Hon, Thin Solid Films 416 (2002) 31–37.
[26] T. Homma, I. Komatsu, A. Ttamaki, H. Nakai, T. Osaka, Electrochimica Acta 47 (2001) 47–53.
[27] M. Palaniyappa, S.K. Seshadri, Journal of Materials Science 42 (2007) 6600–6606.
[28] A. Aal, H.B. Hassan, M.A. Abdel Rahim, Journal of Electroanalytical Chemistry 619 (2008) 17–25.
[29] Q. Zhao, Y. Liu, E.W. Abel, Materials Chemistry and Physics 87 (2004) 332–335.
[30] K.H. Hur, J.H. Jeong, D.N. Lee, Journal of Materials Science 26 (1991) 2037–2044.
[31] N. Krasteva, V. Fotty, S. Armyanov, Journal of Electrochemical Society 141 (1994) 2864–2867.
[32] T. Rabizadeh, S.R. Allahkaram, Materials and Design 32 (2011) 133–138.
[33] C.H. Stoessel, J.C. Withers, C. Pan, D. Wallace, R.O. Loutify, Surface and Coatings Technology 76–77 (1995) 640–644.
[34] C.H. Hager Jr., J. Sanders, S. Sharma, A.A. Voevodin, Wear 267 (2009) 1470–1481.
[35] Y. Wu, B. Shen, L. Liu, W. Hu, Wear 261 (2006) 201–207.
[36] Y.T. Wu, L. Lei, B. Shen, W.B. Hu, Surface and Coatings Technology 201 (2006) 441–445.
[37] M. Ghorbani, M. Mazaheri, K. Khangholi, Y. Kharazi, Surface and Coatings Technology 148 (2001) 71–76.
[38] T. Nickchi, M. Ghorbani, Surface and Coatings Technology 203 (2009) 3037–3043.
[39] M. Ghorbani, M. Mazaheri, A. Afshar, Surface and Coatings Technology 190 (2005) 32–38.
[40] E. Hollingsworth, H. Hunsicker, Metals Handbook, nineth ed., vol. 13, ASM International, 1987, pp. 583–609.
[41] R. Kaibyshev, F. Musin, D.R. Lesuer, T.G. Nieh, Materials Science Engineering A 342 (2003) 169–177.
[42] C.K. Lee, Surface and Coatings Technology 202 (2008) 4868–4874.
[43] C. Gu, J. Lian, G. Li, L. Niu, Z. Jiang, Journal of Alloys and Compounds 391 (2005) 104–109.
[44] N. Guglielmi, Journal of Electrochemical Society 119 (1972) 1009–1012.
[45] J.N. Balaraju, K.S. Rajam, International Journal of Electrochemical Science 2 (10) (2007) 747–761.
[46] A. Robin, R.O. Fratari, Journal of Applied Electrochemistry 37 (2007) 805–812.
[47] U.S. Department of Energy Website. http://www1.eere.energy.gov/hydrogenandlfuelcells/mypp/, 2012, Section 3.4, p. 29.
[48] S.J. Lee, C.H. Huang, Y.P. Chen, Journal of Materials Processing Technology 140 (2003) 688–693.
[49] A. Abdel Aal, Materials Science Engineering A 474 (2008) 181–187.